Environmental Science & Technology

pubs.acs.org/est

Article

Structure–Energetics–Property Relationships Support Computational Design of Photodegradable Pesticides

Jessica Lewer, Jessica Huang, John Peloquin, and Jakub Kostal*

Cite This: *Environ. Sci. Technol.* 2021, 55, 11713–11722

Read Online

ACCESS | Metrics & More | Article Recommendations | Supporting Information

ABSTRACT: Development of high-performing pesticides with tunable degradation properties is vital to increasing the safety and effectiveness of tomorrow's analogs. Chromophoric dissolved organic matter in the excited triple state (^{3}CDOM*) is known to play a key role in the removal of pesticides via indirect photodegradation. However, the potential of these transformations to guide the design of safer chemicals has not yet been fully realized. Here, we report a two-tier computational framework developed to probe and predict both kinetics and thermodynamics of ^{3}CDOM*-pesticide interactions. In the first tier, robust *in silico* models were constructed by fitting free energies obtained from density functional theory (DFT) calculations to cell potentials and second-order rate constants for the ^{3}CDOM*-pesticide electron transfer. In the second tier, Gibbs free energies and corresponding free energy barriers, determined in solution using the Marcus theory, were applied to develop a quick yet accurate screening approach based on the frontier molecular orbital (FMO) Theory. Being highly mechanistic and spanning ca. 1500 unique ^{3}CDOM*-pesticide interactions, our approach is both robust and broadly applicable. To that end, the outcomes of our computational models were integrated into an easy-to-use decision framework that can guide structure-based design of less persistent pesticide analogs.

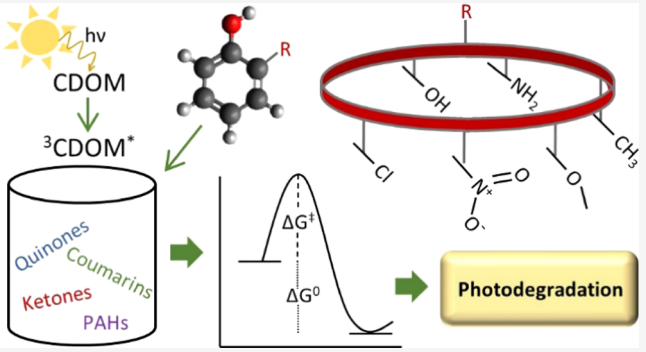

KEYWORDS: *photodegradation, pesticides, chromophoric dissolved organic matter, computational, frontier molecular orbital theory*

INTRODUCTION

Design of high-performing pesticides that pose minimal adverse effects to the environment is among the grand challenges of green chemistry. As the size of the world's population continues to grow, so does the global crop demand and use of pesticides.[1] Since 2007, the global cost-to-benefit ratio of pesticide use has declined due to overuse, persistence, and associated negative environmental effects.[1] Despite regulatory emphasis that pesticides should not persist beyond their intended period of use, approximately half of detected pesticides have long been phased out of use, and another 10–20% are stable transformation products.[2] Health and environmental risk are a function of pesticide toxicity (hazard) and exposure. Pesticide persistence can lead to an increased hazard via the generation of toxic metabolites or increased exposure via increased lifetime in the environment, both of which will subsequently elevate the risk.[3] Presently, degradation is the only method of pesticide removal after use and is therefore a critical metric to target in safer pesticide design.[2] Degradation of pesticides occurs via biotic and abiotic processes. While biotic processes vary based on environmental conditions, photochemical (abiotic) processes are ubiquitous. Photo-transformations occur directly, via absorption of light, or indirectly, via reactions with photochemically produced reactive intermediates (PPRIs). Chromophoric dissolved organic matter in its (excited) triplet state (^{3}CDOM*) is the most ubiquitous class of PPRIs known to degrade pesticides and pharmaceuticals in the environment.[4−6]

A ^{3}CDOM* is formed by photochemical excitation of a ground state (GS) to a short-lived singlet state (^{1}CDOM*), which decays to the more stable triplet state (Figure 1).[7−9] In the environment, ^{3}CDOM* exists as a mixture of mostly ketone and aldehyde sensitizers,[10] which are known to oxidize anilines[11] and phenols,[12−15] ubiquitous cores of many agrochemicals.[16−21] Oxidation occurs via an electron transfer (ET) coupled with, or followed by, a proton transfer.[13,22] A representative, single-electron transfer between a ketone ^{3}CDOM* and a pesticide, which proceeds via an intermediate complex, is shown in Scheme 1.

Canonica et al. reported weak kinetic isotope effects for oxidation of phenols via ^{3}CDOM*, which supports the two-

Received: April 19, 2021
Revised: August 10, 2021
Accepted: August 11, 2021
Published: August 24, 2021

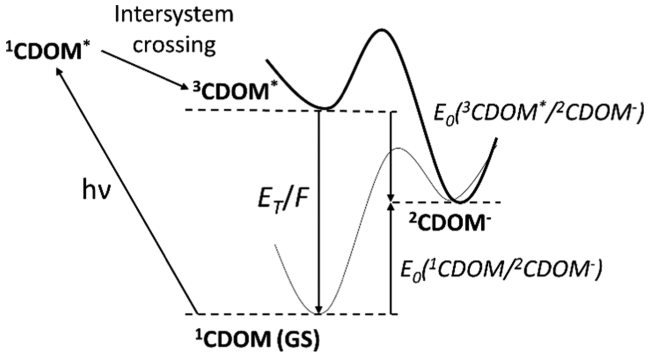

Figure 1. Schematic representation of the excitation and reduction processes of CDOM considering its ground state (GS) and excited singlet (^{1}CDOM*) and triplet (^{3}CDOM*) states.

Scheme 1. Representative ^{3}CDOM*-Pesticide Single-Electron Transfer Reaction

$$\text{Pest} + {}^3(R_1R_2\text{-C=O})^* \leftrightarrows [\text{Pest}\cdots{}^3(R_1R_2\text{-C=O})^*] \leftrightarrows [\text{Pest}^{\bullet+}\cdots R_1R_2\text{-C}^{\bullet}\text{-O}^-] \rightarrow \text{Pest}^{\bullet+} + R_1R_2\text{-C}^{\bullet}\text{-O}^-$$

step electron transfer process over a proton-coupled mechanism.[13] Thus, an electron transfer from the pesticide to the ^{3}CDOM* initiates the degradation process, followed by a downhill, i.e., effectively barrier-less, proton transfer. To that end, the energetics of the electron transfer can serve as an indicator of the indirect photodegradation potential. From Figure 1, in considering substrate oxidation by ^{3}CDOM*, the triplet state reduction potential of CDOM, $E_0(^3\text{CDOM}^*/^2\text{CDOM}^-)$, and the oxidation potential of the substrate pesticide, $E_0(^1\text{Pest}/^2\text{Pest}^+)$, drive the thermodynamics of photodegradation, while the transition state of the association complex informs the process kinetics. In addition to phenols and anilines, some sulfur-containing compounds and alkyl amines have been shown to react with ^{3}CDOM*;[12,23−26] however, their mechanisms are not completely understood. Mechanistic understanding is also lacking for polyfunctional compounds, such as atorvastatin or amoxicillin.[27,28]

Current experimental methods for probing pesticide phototransformations suffer from being costly, difficult to execute, and potentially unreliable for representing multiple substrates.[29−31] To that end, these methods have offered limited insight into the structure−property relationships between various CDOMs/pesticides, which is needed to facilitate the design of pesticides with desirable environmental-fate metrics. On the other hand, *in silico* models represent a cost-effective way of accurately describing the redox chemistry involved, as shown by Pavitt et al.[32] Here, we report a tiered computational framework based on density functional theory (DFT), developed to both quickly and accurately probe kinetics and thermodynamics of the ^{3}CDOM*-pesticide electron transfer. Our approach stems from prior successful initiatives in developing property- and activity-driven design guidelines to aid in lignin and cellulose dissolution in biomass deconstruction[33] as well as to inform both human- and eco-toxicity of various chemical classes.[34−39] The results of this study can be used directly to make predictions based on the electronic structure of pesticides' active ingredients; assess alternatives using common products as a benchmark; and aid chemists with the design of new pesticide analogs with desirable photodegradation metrics. In contrast to traditional (quantitative) structure−activity and property relationships, (Q)SAR/(Q)SPR, our approach is unique in that it fills experimental data gaps with a rigorous reaction-energetics approach to address a broader chemical space in structure-based design.

METHODS

A two-tier computational approach (Figure 2), based on a proven strategy in structure−energetics design,[33] was developed to provide both accurate and broadly applicable predictions of pesticide photodegradation kinetics and thermodynamics. In Tier 1, free energies for the pesticide-to-^{3}CDOM* electron transfer were computed and fit to experimental metrics, while in Tier 2, we focused on fitting computationally-inexpensive electronic parameters, derived solely from the pesticide and ^{3}CDOM* structures, to reaction-pathway energetics. This two-tier approach facilitates robust expansion of the model's training set beyond existing experimental data.[33]

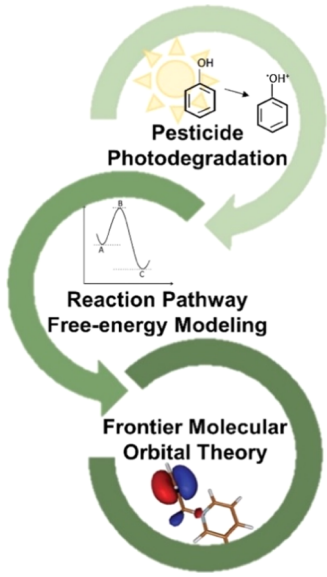

Figure 2. Two-tier computational approach for predicting photodegradation and informing the design of new pesticides.

Experimental data used in our models were collected from reports by Canonica et al.[40] and Pavitt et al.,[32] yielding a total of 23 CDOM structures and 63 pesticide cores (Tables S1 and S2). The resultant dataset consisted of reliable redox thermodynamics (reduction, oxidation, and cell potentials, with experimental error = ±0.02 V) and, for a subset of three CDOMs and nine pesticides, also redox kinetics (second-order rate constants, with experimental error log k = ±0.01−0.30).

Initially, DFT calculations at the M06-2X/6-311+G(3df,3pd) level of theory were used to probe the correlations between computed free energies and experimental cell potentials, $E_{cell}^0 = (E_{red} - E_{ox})$, relying on the Nernst equation, $\Delta G = -nF\,E_{cell}^0$. The M06-2X functional[41] was selected based on reliable performance in describing electron-transfer processes in previous studies.[32] While a large basis set was critical in establishing a dependable benchmark, in optimizing our computational approach for the entire dataset, we found a medium-size basis set, 6-31+G(d,p), offered comparable accuracy at ca. 10% of the computational cost. To better

https://doi.org/10.1021/acs.est.1c02556
Environ. Sci. Technol. 2021, 55, 11713−11722

mimic experimental and real-world conditions, the implicit solvent model based on density (SMD) was used to gauge solvent effects on computed energetics and their correlations to thermodynamic and kinetic data.[42]

For most chemical reactions, there is no discernible relationship between ΔG_{rxn} and $\Delta G^{\ddagger}$; however, a few exceptions exist, including single-electron transfer processes. For these reactions, the dependence of second-order rate constants, k_{et}, on ΔG_{et}^{0} can be described by the Marcus theory. In Marcus theory, the solvent and solute contribution in the electron transfer (ET) process is quantified by the reorganization energy, λ, which can be interpreted as the Gibbs free energy reflective of bond and solvent reorganization needed to alter the structure of solvated reactants to match that of solvated products before the ET (Figure 3).

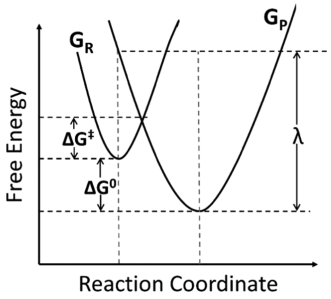

Figure 3. Reaction Coordinate diagram for the electron transfer process. ΔG^{0} is the thermodynamic free energy; $\Delta G^{\ddagger}$ is the free energy barrier; and λ is the solvent reorganization energy. The labels G_R and G_P refer to the reactant and products states, respectively.

To that end, both ΔG_{et}^{0} and λ can be related to the activation energy of the electron transfer as

$$\Delta G^{\ddagger} = w + \frac{(\lambda + \Delta G_{et}^{0})^2}{4\lambda} \quad (1)$$

where w is the electrostatic work done to bring reactants together to form the donor−acceptor association complex, i.e., the ^{3}CDOM*-pesticide intermediate. In our estimations of $\Delta G^{\ddagger}$, λ was computed as a measure of the structural change between ionic and neutral states, which can be expressed for electron (λ_e) and hole (λ_h) by considering optimized neutral, cationic, and anionic geometries

$$\lambda_e = (E_0^- - E_-^-) + (E_-^0 - E_0^0)$$
$$\lambda_h = (E_0^+ - E_+^+) + (E_+^0 - E_0^0) \quad (2)$$

where E_0^+/E_0^- is the energy of the cation/anion calculated with the optimized structure of the neutral molecule; E_+^+/E_-^- is the energy of the cation/anion calculated with the optimized cation/anion structure; E_+^0/E_-^0 is the energy of the neutral molecules computed at the cationic/anionic state; and E_0^0 is the energy of the neutral structure at the ground state.[44,45] The components of λ are additive, and thus eq 2 can be readily applied to evaluate $\Delta G^{\ddagger}$ using eq 1. The electrostatic work term, w, was ignored in our calculations due to the conformationally ambiguous nature of the intermediate complex, which would require an expensive sampling method and dispersion correction to assess accurately, and due to satisfactory performance of the current approach (viz. Results and Discussion).

In Tier 2, ΔG_{et}^{0} and $\Delta G^{\ddagger}$ values were used to gauge the applicability and performance of reactant-based electronic properties derived from the frontier molecular orbital (FMO) theory. Pioneered by Kenichi Fukui, the FMO theory has long served as a simple measure of thermodynamic and kinetic stability.[46] An extension of the highest occupied molecular orbital-lowest unoccupied molecular orbital (HOMO-LUMO) concept was applied here to evaluate properties such as band gap, softness, hardness, and electrophilicity, based on the HOMO(pesticide) and SOMO(^{3}CDOM*) energies (Table 1). We should note that ^{3}CDOM* involves two singly occupied molecular orbital (SOMO) energy levels: the higher-energy SOMO electron acts as a reductant, whereas the lower-energy SOMO electron hole functions as an oxidant. In the Pesticide-^{3}CDOM* ET, ^{3}CDOM* acts as an oxidant; thus, the lower-energy SOMO was used in calculations outlined in Table 1. Orbital energies were calculated at the mPW1PW91/MIDIX+ level of theory, which was developed to yield accurate energies of occupied and virtual frontier orbitals while being relatively inexpensive (<50% of computational time required for 6-31+G(d,p) calculations with the same functional).[48] Our previous studies have shown this approach to be a strong performer in predicting both experimental outcomes and in correlating FMO energies to computed reaction energetics.[33,49] All electronic structure calculations were carried out using the Gaussian 16 program.[43] For additional computational details and parameters explored in this study, see corresponding Supporting Information (SI-1).

Table 1. Electronic Properties Derived from Frontier Molecular Orbitals (FMOs) Tested in This Study for their Correlations with Computed ΔG_{et}^{0} and $\Delta G^{\ddagger}$ Values[a,47]

electronic property	definition	computational approach
band gap (^{3}CDOM*-Pest), ΔE	$\Delta E = E_{SOMO} - E_{HOMO}$	E_{SOMO} (^{3}CDOM*) − E_{HOMO}(Pest)
chemical potential, μ	$\mu = -\chi = \left(\frac{\partial E}{\partial N}\right)_{\nu(r)}$	$\frac{E_{SOMO} + E_{HOMO}}{2}$
chemical hardness, η	$\eta = \left(\frac{\partial^2 E}{\partial N^2}\right)_{\nu(r)} = \left(\frac{\partial \mu}{\partial N}\right)_{\nu(r)}$	$\frac{E_{SOMO} - E_{HOMO}}{2}$
chemical softness, S	$S = 1/\eta$	$\frac{2}{E_{SOMO} - E_{HOMO}}$
chemical electrophilicity, ω	$\omega = \frac{\mu^2}{2\eta}$	$\frac{(E_{HOMO})^2 + 2(E_{HOMO})(E_{SOMO}) + (E_{SOMO})^2}{4(E_{SOMO} - E_{HOMO})}$

[a] ^{3}CDOM* = triplet state chromophoric dissolved organic matter, HOMO = highest occupied molecular orbital, SOMO = singly occupied molecular orbital, Pest = pesticide, χ = electronegativity, ν = external potential, E = energy, N = number of electrons.

https://doi.org/10.1021/acs.est.1c02556
Environ. Sci. Technol. 2021, 55, 11713−11722

RESULTS AND DISCUSSION

Univariate Models. In Tier 1 of our computational approach (Figure 2), we explored the relationship between free energies (ΔG_{et}^{0} and $\Delta G^{\ddagger}$) of the ^{3}CDOM*-pesticide ET and experimentally-derived oxidation/reduction potentials and second-order rate constants. Initial calculations at the M06-2X/6-311+G(3df,3pd) level of theory in the gas phase showed that both computed and experimental reduction and oxidation potentials were well-correlated (R^2 = 0.84 for three CDOMs and nine pesticides, viz. Figure S1). Free energy barriers, $\Delta G^{\ddagger}$'s, estimated from the Marcus theory (eq 1) with implicit solvation (SMD) showed a slightly lower correlation to second-order rate constants, though the overall fit was still very good (R^2 = 0.75, Figure S2).

To improve the model, we searched for outliers in the pesticide-^{3}CDOM* interactions, with residuals greater than two standard deviations from the regression line. Across the 24 pairwise interactions, the ET between 2-acetylnaphthalene and tyrosine fits such description. For this interaction, the log k value was underestimated by our linear model, likely due to the greater selectivity of 2-acetylnapthenone over benzophenone and 3-methoxyacetophenone sensitizers.[40] Removing this outlier increased the coefficient of determination from 0.75 to 0.79 (Figure 4), while also decreasing the root-mean-square

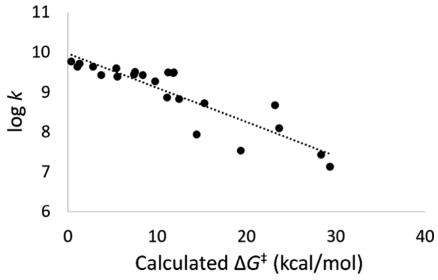

Figure 4. Linear model based on a correlation between experimental log k values and computed free energy barriers, $\Delta G^{\ddagger}$, with an outlier (2-acetylnaphthalene /Tyrosine interaction) removed. R^2 = 0.79, log k = −0.09 × $\Delta G^{\ddagger}$ + 9.95, p-value = 1.28 × 10^{-8}, RMSE = 0.37, q^2 = 0.77, and N = 23.

error (RMSE = 0.37). To assess the predictive power of the linear model in Figure 4, we used the leave-one-out method, i.e., leaving out 10% of the data to create a test set, which yielded q^2 of 0.77, indicating a robust model. For completeness, we should note that correlations of ΔG_{et}^{0}'s (without reorganization energy, λ) to rate constants were expectedly worse (R^2 = 0.68 and 0.41 for linear models with and without implicit solvation, respectively).

In expanding our computational protocol to a larger dataset, it was necessary to combine studies that used two different methods for determining oxidation potentials, namely pulse radiolysis[40] and square wave voltammetry.[32,50]

Thus, an empirical correction factor was developed to standardize E_{ox} and E_{cell}^{0} values using a linear regression analysis for six phenols that overlapped between the studies (Figure S3). Empirically corrected energetics markedly improved the performance in the expanded dataset, which contained 63 pesticides (phenol, aniline, aryl ether, indole, and sulfide cores), and 23 CDOMs, for a total of 1449 pairwise interactions. From Figure 5, computed ΔG_{et}^{0}'s and cell potentials, E_{cell}^{0} (E_{red} − E_{ox}), were well-correlated (R^2 = 0.72), and the linear model was found to be robust and

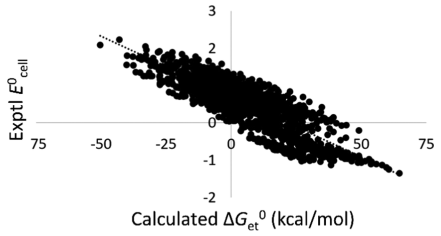

Figure 5. Linear model based on a correlation between experimental cell potentials, E_{cell}^{0} = (E_{red} − E_{ox}) and free energies, ΔG_{et}^{0}, computed at the SMD-M06-2X/6-31+G(d,p) level of theory. Empirical corrections were applied to all chemical classes except anilines. R^2 = 0.72, E_{cell}^{0} = −0.03 × ΔG_{et}^{0} + 0.70, p-value = 0.0, RMSE = 0.35, q^2 = 0.72, and N = 1449.

predictive (q^2 = 0.72). Combining all pesticides and CDOMs into a universal linear model has the advantage of broader applicability and is particularly useful when addressing naturally occurring CDOM mixtures. However, Figure 5 shows there are distinct trends within clusters of pairwise interactions. To that end, we note that performance metrics can be improved in models based on pesticides' oxidizable core (Figure S4).

In Tier 2 of our computational approach, we applied the FMO theory to probe the relationship between electronic parameters derived from HOMO(pesticide) and SOMO-(^{3}CDOM*) energies and free energies, ΔG_{et}^{0}'s. The HOMO-(Pest)-SOMO(^{3}CDOM*) energy gap (ΔE) based on restricted open-shell DFT (RODFT) calculations emerged as the strongest performer (R^2 = q^2 = 0.85, viz. Figure S5). In our analysis, RODFT outperformed unrestricted DFT (UDFT) by ca. 0.2−0.3 in R^2 values across all models, likely due to spin-contamination issues (viz. Supporting Information, SI-1). In contrast to Tier 1, we found that pesticide-core-specific models did not, on average, outperform the universal model; however, most models partitioned by both pesticide class and CDOM showed remarkable correlations to ΔG_{et}^{0}'s (R^2 ∼ 0.94−0.99, Table S3). In the universal linear model, two ^{3}CDOM* molecules, acetophenone and benzophenone, were responsible for 55 of the 74 identified outliers (Figure S5). These two sensitizers had the two lowest SOMO energies in the dataset (−5.29 and −5.25 eV, respectively), indicating small band gaps and, by extension, overly favorable ΔG_{et}^{0} values. In considering an applicability domain based on a −5.25 eV cutoff for E_{SOMO}, these outliers were removed, increasing the performance of both the universal model and pesticide-class-specific models by a significant margin (Figure 6).

The FMO approach was also studied for its utility in predicting computed $\Delta G^{\ddagger}$ values, arguably the more important determinants of indirect photodegradation. A second-order polynomial trend was identified between $\Delta E_{HOMO\text{-}SOMO}$ values and $\Delta G^{\ddagger}$'s in the universal model (Figure S6, top left). Partitioning the model by pesticide class revealed several notable outliers across all 1449 interactions (Figure S6). The largest outliers were under-predicted in our $\Delta G^{\ddagger}$−ΔE models and comprised interactions between unfunctionalized poly-aromatic hydrocarbons (PAHs), such as anthracene, pyrene, naphthalene and phenanthrene, and pesticides with high oxidation potentials, particularly 4-nitroaniline and dimethyl-sulfide (Figure S6). Having the lowest reduction potentials of all of the CDOM in our dataset (0.15−0.46), PAHs should be treated in a separate model, given the well-known limitations of small basis sets in predicting energies of highly-delocalized

https://doi.org/10.1021/acs.est.1c02556
Environ. Sci. Technol. 2021, 55, 11713−11722

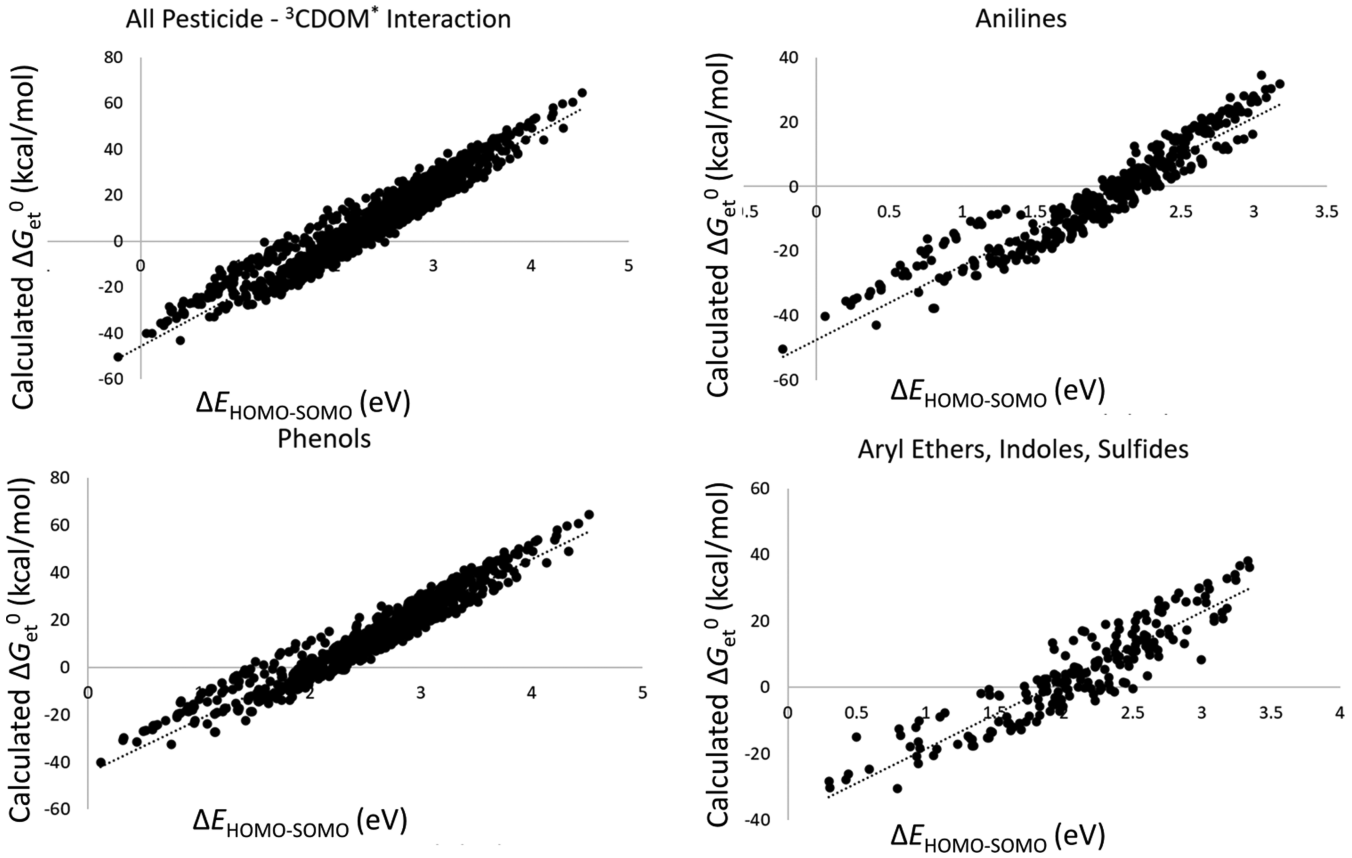

Figure 6. Linear models based on correlations between HOMO-SOMO energy gap, $\Delta E_{\text{HOMO-SOMO}}$ and free energies, ΔG_{et}^{0}, computed at the SMD-ROmPW1PW91/MIDIX+ level of theory. Top left: $R^2 = 0.91$, $\Delta G_{et}^{0} = 22.83 \times \Delta E - 45.51$, p-value = 0.0, RMSE = 5.21, $q^2 = 0.92$, and $N = 1325$. Top right: $R^2 = 0.90$, $\Delta G_{et}^{0} = 22.92 \times \Delta E - 47.38$, p-value = 4.4×10^{-194}, RMSE = 5.00, $q^2 = 0.89$, and $N = 394$. Bottom left: $R^2 = 0.92$, $\Delta G_{et}^{0} = 22.63 \times \Delta E - 44.67$, p-value = 0.0, RMSE = 4.89, $q^2 = 0.92$, and $N = 734$. Bottom right: $R^2 = 0.84$, $\Delta G_{et}^{0} = 20.66 \times \Delta E - 39.19$, p-value = 2.93×10^{-80}, RMSE = 7.27, $q^2 = 0.85$, and $N = 198$.

FMOs.[49] In using this criterion to define the models' applicability domain, all relevant 70 pairwise interactions were removed, yielding a robust universal model ($R^2 = q^2 = 0.92$, Figure 7) and improved class-specific models ($R^2 =$ 0.86–0.92, Figure S7). As noted for the $\Delta G_{et}^{0} - \Delta E$ models, correlations based on individual CDOMs outperformed the universal model ($R^2 > 0.97$).

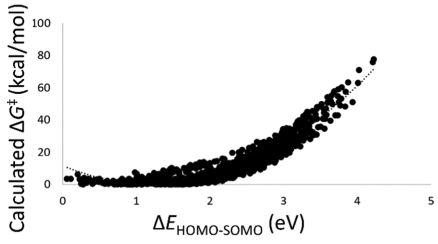

Figure 7. Univariate model based on a second-order polynomial correlation between $\Delta E_{\text{HOMO-SOMO}}$ and free energy barriers, $\Delta G^{\ddagger}$, computed at the SMD-ROmPW1PW91/MIDIX+ level of theory. $R^2 = 0.92$, $\Delta G^{\ddagger} = 7.81 \times (\Delta E)^2 - 18.79 \times \Delta E + 11.59$, p-value = 3.5×10^{-193}, RMSE = 3.38, $q^2 = 0.92$, and $N = 1402$.

Design Implications. The two-tier approach developed here indicates that both thermodynamic and kinetic data for pesticide degradation by ^{3}CDOM* can be reliably derived from univariate models based on HOMO(Pest)-SOMO-(^{3}CDOM*) energy gap, $\Delta E_{\text{HOMO-SOMO}}$. While models based on pairwise interactions can be used to quickly screen novel pesticides of interest, it is important to consider the general ability of individual ^{3}CDOM*s to oxidize these chemicals. Such analysis provides insight into the relative importance of the components of naturally occurring ^{3}CDOM* mixtures. To that end, second-order rate constants, log k's, were computed across the 23 CDOMs and 63 pesticide cores relative to the commonly studied combination of 3-methoxyacetophenone (3MAP) and 2,4,6-trimethylphenol (TMP). Due to the ambiguous nature of CDOM, sensitizers such as 3MAP are used as molecules representative of the complex mixture, and TMP is frequently employed as a pesticide probe in photodegradation studies.[10] In Figure 8, the TMP-3MAP interaction was set to log $k = 1$, and all other interactions were scaled accordingly. We found that CDOM-makeup can alter the average relative log k's by as much as a 1.5-fold from the population (i.e., 1449 interactions') mean. This large variation points to the need to steer the design of novel pesticides toward compounds that are less impacted by CDOM composition in their ability to break down.

In examining pesticide sensitivity to CDOM mixture, pesticide cores were evaluated for their kinetic susceptibility to undergo oxidation by ^{3}CDOM* across all 23 sensitizers (Figure S8). A subset containing all primary (non-substituted) cores as well as compounds with the two highest and two lowest log k values is shown in Figure 9.

https://doi.org/10.1021/acs.est.1c02556
Environ. Sci. Technol. 2021, 55, 11713–11722

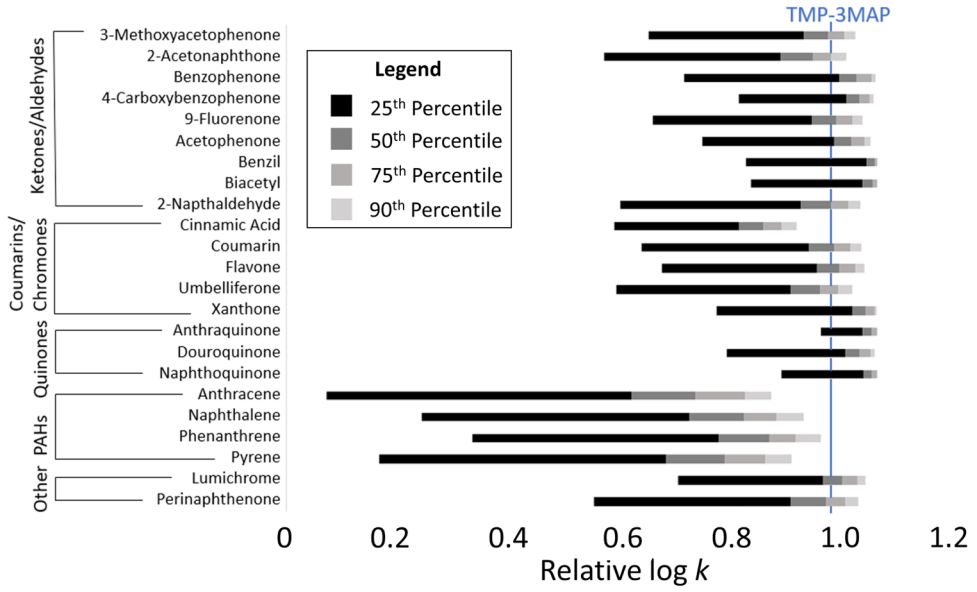

Figure 8. Relative log of the computed second-order rate constant (per CDOM across all 63 pesticide cores). The left-most edge of the bar represents the minimum value; the right-most edge of each shading from darkest to lightest represents the 25th, 50th, 75th, and 90th percentiles, respectively. Reference log k = 1, corresponding to the 2,4,6-trimethylphenol (TMP) − 3-Methoxyacetophenone (3MAP) interaction, is shown in blue.

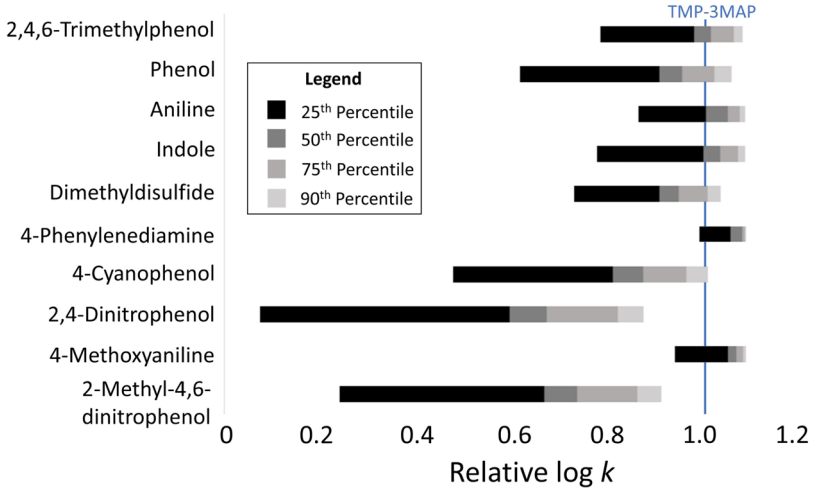

Figure 9. Distributions of relative log k values across 23 CDOMs for a subset of 9 pesticide cores. The left-most edge of the bar represents the minimum value; the right-most edge of each shading from darkest to lightest represents the 25th, 50th, 75th, and 90th percentiles, respectively. Reference log k = 1, corresponding to the 2,4,6-trimethylphenol (TMP) − 3-Methoxyacetophenone (3MAP) interaction, is shown in blue.

In principle, an ideal core would not only possess a high average rate constant, increasing the chance of indirect photodegradation after use, but also a narrow range, indicating low susceptibility to fluctuations in CDOM character.[10] From Figure 9, 4-phenylenediamine had the highest average relative rate constant (1.07) with the narrowest distribution, indicating the lowest susceptibility to CDOM composition. In contrast, 2,4-dinitrophenol showed the lowest average relative rate constant (0.65) and high susceptibility to CDOM character. Performed across all 63 pesticide cores (Figure S8), this comparative analysis can be leveraged to inform the design of novel analogs based on existing pesticide cores.

To further illustrate how our model could be used to design pesticides with predictable degradability in natural CDOM mixtures, the 23 sensitizers were combined in ratios that mimic environmental samples. While the precise CDOM content remains elusive and variable, a report by McNeil et al. showed that, on average, high-energy ^{3}CDOM* molecules make up roughly 37% of the total triplet pool; and that ketones, aldehydes, coumarins, and chromones account for most of these high-energy states.[10] To that end, a hypothetical CDOM mixture was created containing ca. 20% ketones/aldehydes and 20% coumarins/chromones, with the remaining 60% evenly split between quinones and PAHs. Since phenols were the most represented class of pesticides in our dataset (Table S1), phenol-^{3}CDOM*(mixture) energetics, relative to the TMP-3MAP interaction, were explored to demonstrate the underlying structure−energetics relationships. In Figure 10, we briefly consider the effect of two common substituents in pesticide products (methoxy and nitro groups) on computed energetics.

https://doi.org/10.1021/acs.est.1c02556
Environ. Sci. Technol. 2021, 55, 11713−11722

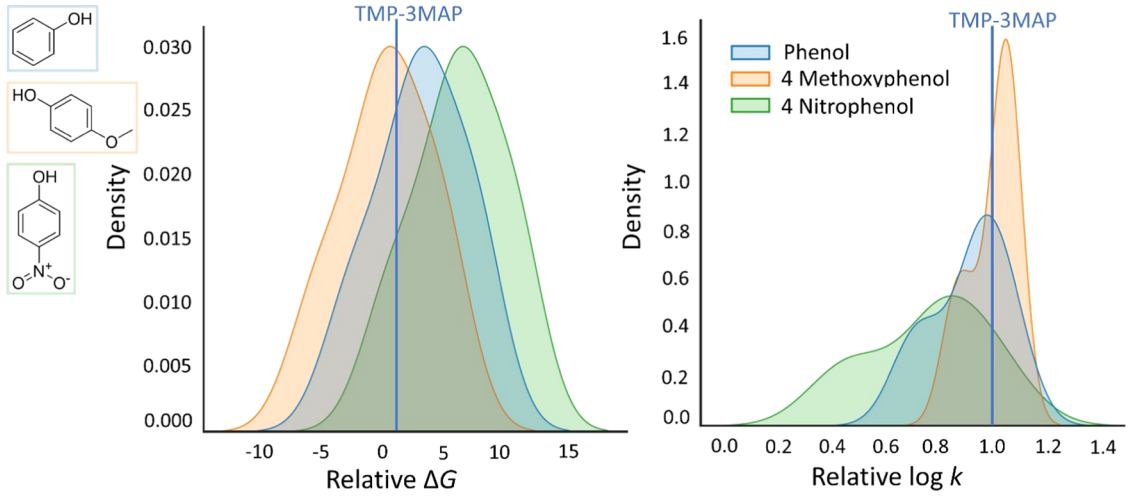

Figure 10. Kernel density plot for distributions of phenol, 4-methoxyphenol, and 4-nitrophenol thermodynamics (ΔG) and kinetics ($\log k$), relative to the 2,4,6-trimethylphenol (TMP) − 3-methoxyacetophenone (3MAP) interaction, when reacted with a hypothetical ^{3}CDOM* mixture containing 20% ketones/aldehydes, 20% coumarins/chromones, 30% quinones, and 30% polycyclic aromatic hydrocarbons.

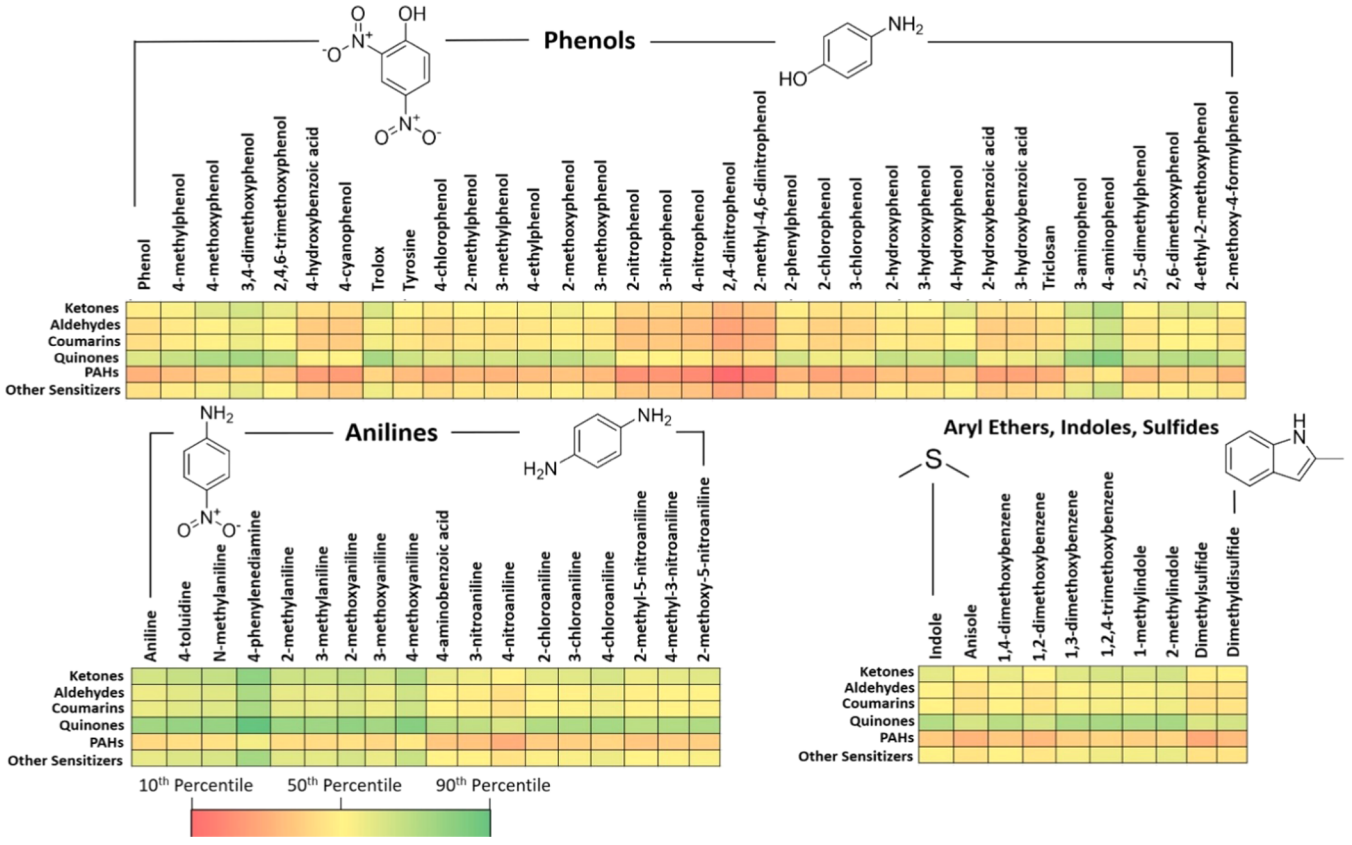

Figure 11. Heat maps of combined kinetic and thermodynamic performance for 1449 pesticide-^{3}CDOM* interactions. Red indicates higher ΔG_{et}^0 values and slower reaction rates, whereas green indicates lower ΔG_{et}^0 values and faster reaction rates. The structures shown represent the least (left) and most (right) reactive cores (averaged across all 23 CDOMs) for each pesticide class.

In this example, we note that the majority of phenol-^{3}CDOM*(mixture) interactions are both thermodynamically and kinetically less favorable than the TMP-3MAP benchmark. While the nitro group results in less favorable interactions than the non-substituted phenol, the methoxy substitution has the opposite effect, leading to faster kinetics and more favorable thermodynamics. This is not surprising, given that the electron-withdrawing nitro group destabilizes the oxidized pesticide radical, while the electron-donating methoxy stabilizes the oxidized form. It is, however, important to note that this propensity is not only captured by the computed $\Delta G^{\ddagger}$'s and ΔG_{et}^0's but also by $\Delta E_{HOMO\text{-}SOMO}$. To that end, our brief analysis demonstrates how the present models could be used to screen existing pesticides and inform structural changes to existing oxidizable cores that would yield the desired effect in the analog's propensity to photodegrade. The merits of redesigning existing chemicals over *de novo* design were explored previously.[37] Subtle structural modifica-

https://doi.org/10.1021/acs.est.1c02556
Environ. Sci. Technol. 2021, 55, 11713−11722

tions are potentially more economically viable because they allow manufacturers to cost-effectively tune existing synthetic routes without the need to develop new chemistries. Furthermore, incremental design changes are less likely to disrupt pesticides' intended function, in turn increasing the likelihood of adopting a safer substitute.

Analyzing each of the 1449 pairwise interactions between pesticides and ^{3}CDOM*, we found that log k's ranged from 1 standard deviation above the TMP-3MAP interaction to 3 standard deviations below (Figure S9), while ΔG_{et}^{0}'s ranged from just over 3 standard deviations above to just under 3 below the TMP-3MAP benchmark (Figure S10). To gain a holistic picture of ET-induced photodegradability across all interactions, a heat map was generated, combining computed kinetics and thermodynamics using percentage values of the relative log k's and ΔG_{et}^{0}'s (Figure 11). Provided CDOMs exist in unspecified mixtures in the natural environment, the 23 sensitizers in Figure 11 were averaged into functional-class bins (*viz.* Table S4). A few general trends emerged from this analysis. Anilines were noted to degrade faster than any other pesticide class. The degradation of phenols was found to be dependent on substituents present in the oxidizable core. Considering CDOM, quinones represent the most reactive class in the photodegradation process, whereas PAHs are the most inert, which is consistent with reported data.[10] We envision this format can facilitate rapid screening of novel pesticides by structure-matching to the most relevant pesticide core explored in this study and identifying photodegradation potential across a wide range of CDOMs.

Outlook. Understanding structure−property relationships that drive the degradation of pesticides in the environment is necessary for developing new, high-performing products with minimal adverse environmental impact. Indirect photodegradation via excited chromophoric dissolved organic matter (CDOM) is among the most ubiquitous natural processes that remove agricultural products from the environment. To that end, *in silico* models based on mechanisms of the relevant redox processes can advance design efforts by identifying novel analogs with desirable degradation properties.

The two-tier computational framework presented here demonstrates how such design guidelines can be developed using structure−energetics−property relationships. By relating rigorous calculations of electron-transfer energetics to electronic properties and subsequently to structures of pesticides and CDOM sensitizers, we can fill data gaps in photodegradation metrics and probe a chemical space that vastly exceeds existing experimental knowledge. The results shown here (Figures 11, S9, and S10) can be directly leveraged to identify pesticide cores and core substituents that have favorable degradation profiles with specific CDOM components, CDOM classes, or environmentally relevant CDOM mixtures. The two-tier approach is advantageous over traditional QSAR/QSPR methods in that it self-generates a broader training set, expanding the model's applicability and predictivity. Inspired by benchmarking practices in computational chemistry, this strategy can be readily extended to other *in silico* design efforts targeting chemical properties and/or activities that relate to performance, toxicity, or environmental transformations, for which we have good mechanistic interpretation.

While promising in guiding pesticide selection and future design efforts, we should recognize that bringing new products to market is a multifaceted challenge that requires systems thinking. To that end, the current work represents but a small step toward a holistic (computational) design strategy, which we envision would expand the redox chemistry to other photochemically produced reactive intermediates (PPRIs); provide insight into degradation pathways; integrate toxicity assessments of all relevant (by)products; and evaluate synthetic feasibility of promising analogs based on proposed structural modifications. Because low persistence does not ensure safety and neither guarantees adequate performance, relevant structural attributes will need to be reconciled in a combined model to inform new product development. This task can be accomplished by extending current and building upon past efforts.[34,35] The resultant tool, when developed, would equip the chemistry community with a pragmatic means of designing all-around safer and high-performing agricultural products.

■ ASSOCIATED CONTENT

Supporting Information

The Supporting Information is available free of charge at https://pubs.acs.org/doi/10.1021/acs.est.1c02556.

Two-dimensional (2D) chemical structures, experimental data, computed energetics, additional linear and nonlinear models, and computed distributions of thermodynamic and kinetic data for each pesticide-^{3}CDOM* pairwise interaction are provided (PDF)

■ AUTHOR INFORMATION

Corresponding Author

Jakub Kostal − *Department of Chemistry, The George Washington University, Washington, District of Columbia 20052-0066, United States;* orcid.org/0000-0001-9727-0477; Email: jkostal@gwu.edu

Authors

Jessica Lewer − *Department of Chemistry, The George Washington University, Washington, District of Columbia 20052-0066, United States*

Jessica Huang − *Department of Chemistry, The George Washington University, Washington, District of Columbia 20052-0066, United States*

John Peloquin − *Department of Chemistry, The George Washington University, Washington, District of Columbia 20052-0066, United States*

Complete contact information is available at: https://pubs.acs.org/10.1021/acs.est.1c02556

Author Contributions

The manuscript was written through the contributions of all authors. All authors have given approval to the final version of the manuscript.

Notes

The authors declare no competing financial interest.

■ ACKNOWLEDGMENTS

Gratitude is expressed to Geetesh Devineni and Preston Griffin for their help with modeling, data analysis, and thought provoking conversations. This work was supported by the National Science Foundation (NSF1943127).

REFERENCES

(1) Zhang, W. J. Global pesticide use: Profile, trend, cost / benefit and more. *Proc. Int. Acad. Ecol. Environ. Sci.* **2018**, *8*, 1−27.

(2) Fenner, K.; Canonica, S.; Wackett, L. P.; Elsner, M. Evaluating Pesticide Degradation in the Environment: Blind Spots and Emerging Opportunities. *Science* **2013**, *341*, 752−758.

(3) Damalas, C.; Eleftherohorinos, I. Pesticide exposure, safety issues, and risk assessment indicators. *Int. J. Environ. Res. Public Health* **2011**, *8*, 1402−1419.

(4) Remucal, C. K. The role of indirect photochemical degradation in the environmental fate of pesticides: a review. *Environ. Sci.: Processes Impacts* **2014**, *16*, 628−653.

(5) Challis, J. K.; Hanson, M. L.; Friesen, K. J.; Wong, C. S. A critical assessment of the photodegradation of pharmaceuticals in aquatic environments: defining our current understanding and identifying knowledge gaps. *Environ. Sci.: Processes Impacts* **2014**, *16*, 672−696.

(6) Yan, S. W.; Song, W. H. Photo-transformation of pharmaceutically active compounds in the aqueous environment: a review. *Environ. Sci.: Processes Impacts* **2014**, *16*, 697−720.

(7) Grebel, J. E.; Pignatello, J. J.; Mitch, W. A. Sorbic acid as a quantitative probe for the formation, scavenging and steady-state concentrations of the triplet-excited state of organic compounds. *Water Res.* **2011**, *45*, 6535−6544.

(8) Peterson, B. M.; McNally, A. M.; Cory, R. M.; Thoemke, J. D.; Cotner, J. B.; McNeill, K. Spatial and Temporal Distribution of Singlet Oxygen in Lake Superior. *Environ. Sci. Technol.* **2012**, *46*, 7222−7229.

(9) Sandvik, S. L. H.; Bilski, P.; Pakulski, J. D.; Chignell, C. F.; Coffin, R. B. Photogeneration of singlet oxygen and free radicals in dissolved organic matter isolated from the Mississippi and Atchafalaya River plumes. *Mar. Chem.* **2000**, *69*, 139−152.

(10) McNeill, K.; Canonica, S. Triplet state dissolved organic matter in aquatic photochemistry: reaction mechanisms, substrate scope, and photophysical properties. *Environ. Sci.: Processes Impacts* **2016**, *18*, 1381−1399.

(11) Canonica, S.; Laubscher, H. U. Inhibitory effect of dissolved organic matter on triplet-induced oxidation of aquatic contaminants. *Photochem. Photobiol. Sci.* **2008**, *7*, 547−551.

(12) Boreen, A. L.; Edhlund, B. L.; Cotner, J. B.; McNeill, K. Indirect photodegradation of dissolved free amino acids: The contribution of singlet oxygen and the differential reactivity of DOM from various sources. *Environ. Sci. Technol.* **2008**, *42*, 5492−5498.

(13) Canonica, S.; Jans, U.; Stemmler, K.; Hoigne, J. Transformation Kinetics of Phenols in Water - Photosensitization by Dissolved Natural Organic Material and Aromatic Ketones. *Environ. Sci. Technol.* **1995**, *29*, 1822−1831.

(14) Aguer, J. P.; Tetegan, D.; Richard, C. Humic substances mediated phototransformation of 2,4,6-trimethylphenol: a catalytic reaction. *Photochem. Photobiol. Sci.* **2005**, *4*, 451−453.

(15) Halladja, S.; Ter Halle, A.; Aguer, J. P.; Boulkamh, A.; Richard, C. Inhibition of humic substances mediated photooxygenation of furfuryl alcohol by 2,4,6-trimethylphenol. Evidence for reactivity of the phenol with humic triplet excited states. *Environ. Sci. Technol.* **2007**, *41*, 6066−73.

(16) Zeng, T.; Arnold, W. A. Pesticide Photolysis in Prairie Potholes: Probing Photosensitized Processes. *Environ. Sci. Technol.* **2013**, *47*, 6735−6745.

(17) Gerecke, A. C.; Canonica, S.; Muller, S. R.; Scharer, M.; Schwarzenbach, R. P. Quantification of dissolved natural organic matter (DOM) mediated phototransformation of phenylurea herbicides in lakes. *Environ. Sci. Technol.* **2001**, *35*, 3915−3923.

(18) Canonica, S.; Hellrung, B.; Muller, P.; Wirz, J. Aqueous oxidation of phenylurea herbicides by triplet aromatic ketones. *Environ. Sci. Technol.* **2006**, *40*, 6636−6641.

(19) Langlois, M. C.; Weavers, L. K.; Chin, Y. P. Contaminant-mediated photobleaching of wetland chromophoric dissolved organic matter. *Environ. Sci.: Processes Impacts* **2014**, *16*, 2098−2107.

(20) Karpuzcu, M. E.; McCabe, A. J.; Arnold, W. A. Phototransformation of pesticides in prairie potholes: effect of dissolved organic matter in triplet-induced oxidation. *Environ. Sci.: Processes Impacts* **2016**, *18*, 237−245.

(21) Qu, S.; Kolodziej, E. P.; Cwiertny, D. M. Phototransformation Rates and Mechanisms for Synthetic Hormone Growth Promoters Used in Animal Agriculture. *Environ. Sci. Technol.* **2012**, *46*, 13202−13211.

(22) Weinberg, D. R.; Gagliardi, C. J.; Hull, J. F.; Murphy, C. F.; Kent, C. A.; Westlake, B. C.; Paul, A.; Ess, D. H.; McCafferty, D. G.; Meyer, T. J. Proton-Coupled Electron Transfer. *Chem. Rev.* **2012**, *112*, 4016−4093.

(23) Wang, L.; Xu, H. M.; Cooper, W. J.; Song, W. H. Photochemical fate of beta-blockers in NOM enriched waters. *Sci. Total Environ.* **2012**, *426*, 289−295.

(24) Leresche, F.; von Gunten, U.; Canonica, S. Probing the Photosensitizing and Inhibitory Effects of Dissolved Organic Matter by Using N,N-dimethyl-4-cyanoaniline (DMABN). *Environ. Sci. Technol.* **2016**, *50*, 10997−11007.

(25) Chen, Y.; Hu, C.; Hu, X. X.; Qu, J. H. Indirect Photodegradation of Amine Drugs in Aqueous Solution under Simulated Sunlight. *Environ. Sci. Technol.* **2009**, *43*, 2760−2765.

(26) Chen, Y.; Li, H.; Wang, Z. P.; Li, H. J.; Tao, T.; Zuo, Y. G. Photodegradation of selected beta-blockers in aqueous fulvic acid solutions: Kinetics, mechanism, and product analysis. *Water Res.* **2012**, *46*, 2965−2972.

(27) Eskiköy, D.; Durmus, Z.; Kilic, E. Electrochemical Oxidation of Atorvastatin and Its Adsorptive Stripping Determination in Pharmaceutical Dosage Forms and Biological Fluids. *Collect. Czech. Chem. Commun.* **2011**, *76*, 1633−1649.

(28) Hu, X. L.; Liu, J. F.; Lu, S. Y.; Jiang, G. B. Freely Dissolved Concentration and Bioavailability of Environmental Pollutants. *Prog. Chem.* **2009**, *21*, 514−523.

(29) Reemtsma, T.; Alder, L.; Banasiak, U. A multimethod for the determination of 150 pesticide metabolites in surface water and groundwater using direct injection liquid chromatography-mass spectrometry. *J. Chromatogr. A* **2013**, *1271*, 95−104.

(30) Schreglmann, K.; Hoeche, M.; Steinbeiss, S.; Reinnicke, S.; Elsner, M. Carbon and nitrogen isotope analysis of atrazine and desethylatrazine at sub-microgram per liter concentrations in groundwater. *Anal. Bioanal. Chem.* **2013**, *405*, 2857−2867.

(31) Halladja, S.; ter Halle, A.; Pilichowski, J. F.; Boulkamh, A.; Richard, C. Fulvic acid-mediated phototransformation of mecoprop. A pH-dependent reaction. *Photochem. Photobiol. Sci.* **2009**, *8*, 1066−1071.

(32) Pavitt, A. S.; Bylaska, E. J.; Tratnyek, P. G. Oxidation potentials of phenols and anilines: correlation analysis of electrochemical and theoretical values. *Environ. Sci.: Processes Impacts* **2017**, *19*, 339−349.

(33) Griffin, P.; Ramer, S.; Winfough, M.; Kostal, J. Practical guide to designing safer ionic liquids for cellulose dissolution using a tiered computational framework. *Green Chem.* **2020**, *22*, 3626−3637.

(34) Kostal, J.; Voutchkova-Kostal, A.; Anastas, P. T.; Zimmerman, J. B. Identifying and designing chemicals with minimal acute toxicity. *Proceedings Natl. Acad. Sci. U.S.A.* **2015**, *112*, 6289−6294.

(35) Kostal, J.; Voutchkova-Kostal, A.; Weeks, B.; Zimmerman, J. B.; Anastas, P. T. A free energy approach to the prediction of olefin and epoxide mutagenicity and carcinogenicity. *Chem. Res. Toxicol.* **2012**, *25*, 2780−2787.

(36) Steele, W. B.; Kristofco, L. A.; Corrales, J.; Saari, G. N.; Corcoran, E. J.; Hill, B. N.; Mills, M. G.; Gallagher, E.; Kavanagh, T. J.; Melnikov, F.; Zimmerman, J. B.; Voutchkova-Kostal, A.; Anastas, P. T.; Kostal, J.; Brooks, B. W. Toward less hazardous industrial compounds: coupling quantum mechanical computations, biomarker responses, and behavioral profiles to identify bioactivity of SN2 electrophiles in alternative vertebrate models. *Chem. Res. Toxicol.* **2020**, *33*, 367−380.

(37) Clymer, T.; Vargas, V.; Corcoran, E.; Kleinberg, R.; Kostal, J. Redesigning hazardous chemicals by learning from structure-based drug discovery. *Green Chem.* **2019**, *21*, 1935−1946.

https://doi.org/10.1021/acs.est.1c02556
Environ. Sci. Technol. 2021, 55, 11713−11722

(38) Voutchkova, A. M.; Kostal, J.; Steinfeld, J. B.; Emerson, J. W.; Brooks, B. W.; Anastas, P.; Zimmerman, B. Towards rational molecular design: derivation of property guidelines for reduced acute aquatic toxicity. *Green Chem.* **2011**, *13*, 2373−2379.
(39) Voutchkova-Kostal, A. M.; Kostal, J.; Connors, K. A.; Brooks, B. W.; Anastas, P. T.; Zimmerman, J. B. Towards rational molecular design for reduced chronic aquatic toxicity. *Green Chem.* **2012**, *14*, 1001−1008.
(40) Canonica, S.; Hellrung, B.; Wirz, J. Oxidation of phenols by triplet aromatic ketones in aqueous solution. *J. Phys. Chem. A* **2000**, *104*, 1226−1232.
(41) Zhao, Y.; Truhlar, D. G. The M06 suite of density functionals for main group thermochemistry, thermochemical kinetics, noncovalent interactions, excited states, and transition elements: two new functionals and systematic testing of four M06-class functionals and 12 other functionals. *Theor. Chem. Acc.* **2008**, *120*, 215−241.
(42) Marenich, A. V.; Cramer, C. J.; Truhlar, D. G. Universal solvation model based on solute electron density and a continuum model of the solvent defined by the bulk dielectric constant and atomic surface tensions. *J. Phys. Chem. B* **2009**, *113*, 6378−6396.
(43) Frisch, M. J.; Trucks, G. W.; Schlegel, H. B.; Scuseria, G. E.; Robb, M. A.; Cheeseman, J. R.; Scalmani, G.; Barone, V.; Petersson, G. A.; Nakatsuji, H.; Li, X.; Caricato, M.; Marenich, A. V.; Bloino, J.; Janesko, B. G.; Gomperts, R.; Mennucci, B.; Hratchian, H. P.; Ortiz, J. V.; Izmaylov, A. F.; Sonnenberg, J. L.; Williams-Young, D.; Ding, F.; Lipparini, F.; Egidi, F.; Goings, J.; Peng, B.; Petrone, A.; Henderson, T.; Ranasinghe, D.; Zakrzewski, V. G.; Gao, J.; Rega, N.; Zheng, G.; Liang, W.; Hada, M.; Ehara, M.; Toyota, K.; Fukuda, R.; Hasegawa, J.; Ishida, M.; Nakajima, T.; Honda, Y.; Kitao, O.; Nakai, H.; Vreven, T.; Throssell, K.; Montgomery, J. A., Jr.; Peralta, J. E.; Ogliaro, F.; Bearpark, M. J.; Heyd, J. J.; Brothers, E. N.; Kudin, K. N.; Staroverov, V. N.; Keith, T. A.; Kobayashi, R.; Normand, J.; Raghavachari, K.; Rendell, A. P.; Burant, J. C.; Iyengar, S. S.; Tomasi, J.; Cossi, M.; Millam, J. M.; Klene, M.; Adamo, C.; Cammi, R.; Ochterski, J. W.; Martin, R. L.; Morokuma, K.; Farkas, O.; Foresman, J. B.; Fox, D. J.. *Gaussian 16*, revision B.01.; Gaussian, Inc.: Wallingford, CT, 2016.
(44) Stark, M. S. Epoxidation of alkenes by peroxyl radicals in the gas phase: Structure-activity relationships. *J. Phys. Chem. A* **1997**, *101*, 8296−8301.
(45) Sun, F. Y.; Jin, R. F. DFT and TD-DFT study on the optical and electronic properties of derivatives of 1,4-bis(2-substituted-1,3,4-oxadiazole)benzene. *Arabian J. Chem.* **2017**, *10*, S2988−S2993.
(46) Fukui, K.; Yonezawa, T.; Shingu, H. (1952) A molecular orbital theory of reactivity in aromatic hydrocarbons. *J. Chem. Phys.* **1952**, *20*, 722−725.
(47) Kostal, J. Computational chemistry in predictive toxicology: Status quo et quo vadis?. In *Advances in Molecular Toxicology*; Fishbein, J.; Helman, J., Eds.; Elsevier: San Diego, CA, 2016; Vol. *10*, pp 139−186.
(48) Lynch, B.; Truhlar, D. Small basis sets for calculations of barrier heights, energies of reaction, electron affinities, geometries, and dipole moments. *Theor. Chem. Acc.* **2004**, *111*, 335−344.
(49) Kostal, J.; Voutchkova-Kostal, A. CADRE-SS, an in Silico Tool for Predicting Skin Sensitization Potential Based on Modeling of Molecular Interactions. *Chem. Res. Toxicol.* **2016**, *29*, 58−64.
(50) Guerard, J. J.; Arey, J. S. Critical Evaluation of Implicit Solvent Models for Predicting Aqueous Oxidation Potentials of Neutral Organic Compounds. *J. Chem. Theory Comput.* **2013**, *9*, 5046−58.

https://doi.org/10.1021/acs.est.1c02556
Environ. Sci. Technol. 2021, 55, 11713−11722